ACS APPLIED MATERIALS & INTERFACES

Letter

www.acsami.org

Interfacial Reaction-Driven Formation of Silica Carbonate Biomorphs with Subcellular Topographical Features and Their Biological Activity

Guocheng Wang,*[,†] Xiaobing Zhao,[‡] Marco Möller,[§] and Sergio E. Moya[∥]

[†]Research Center for Human Tissues & Organs Degeneration, Shenzhen Institute of Advanced Technology, Chinese Academy of Sciences, Shenzhen, Guangdong 518055, China

[‡]School of Materials Science and Engineering, Changzhou University, 213164 Changzhou, China

[§]EM-Lab and [∥]Soft Matter Nanotechnology Laboratory, CIC biomaGUNE, Paseo Miramón 182 C, 20009 Donostia-San Sebastian, Spain

Supporting Information

ABSTRACT: We report the interfacial reaction-driven formation of micro/nanostructured strontium carbonate ($SrCO_3$) biomorphs with subcellular topographical features on strontium zinc silicate ($Sr_2ZnSi_2O_7$) biomedical coatings and explore their potential use in bone tissue engineering. The resulting $SrCO_3$ crystals build a well-integrated scaffold surface that not only prevents burst release of ions from the coating but also presents nanotopographical features similar to cellular filopodia. The surface with biomorphic crystals enhances osteoblast adhesion, upregulates the alkaline phosphatase activity, and increases collagen production, highlighting the potential of the silica carbonate biomorphs for tissue regeneration.

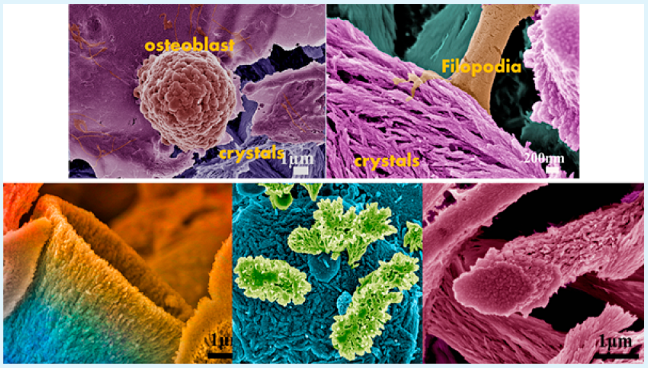

KEYWORDS: *silica biomorph, strontium carbonate, reactivity, osteoblast, bone regeneration*

Recent findings demonstrated that precipitation of alkaline-earth carbonates in silica-rich environments without organic species can yield crystal assemblies with hierarchical structures and shapes.[1−10] These so-called "silica biomorphs" highly resemble the biogenic minerals created by living organisms, arousing a great deal of interest of a wide range of researchers.[1−5] Although many studies have been carried out to study the formation mechanism of the biomorphic crystals, very few explored their practical use. In this letter, we for the first time in situ produced silica−strontium carbonate ($SrCO_3$) biomorphs with well-organized nanostructures on a biomedical coating, aiming for orthopedic applications. Conventional synthesis of a silica biomorph is conducted on an "inert" glass slide substrate in an alkaline sodium silicate gel containing alkaline-earth metal ions. In contrast, the formation of the biomorph in our system is largely dependent on the surface reactivity of a "reactive" substrate, thus driven by interfacial reactions. The newly formed scaffold not only prevents the burst release of ions from the coating but also provides subcellular topographical features, leading to the enhancement of cell adhesion and upregulation of osteoblast functions.

Strontium zinc silicate ($Sr_2ZnSi_2O_7$, hereafter referred to as SZnS) coatings deposited on Ti alloys using a plasma spraying technique on Ti alloy disks were used as the "reactive" substrate for crystal formation in this study. The as-sprayed SZnS coating is composed of partially crystallized $Sr_2ZnSi_2O_7$ (Figure S1). The coating has a ridge (island)-and-valley microstructure surface in which cilia-like nanostructures are embedded (Figure S2). As indicated in Figure 1a,b, the coating has a highly reactive surface that can readily interact with a water-based medium. After incubation for 5 h in a cell culture medium with 10% fetal bovine serum (FBS), foxtail-shaped crystals composed of nanosized fibrous crystallites (building units) were formed on the coating surfaces, as shown in Figure 1a. In the case of incubation in a serum-free cell culture medium, flowerlike crystals are observed to protrude out from the coating surface (Figure 1b), rooted at the nanoscale on the coating surface (Figure 1b, inset).

To get a quick and more efficient manipulation of the chemical reaction on the coating surface, a modified autoclave sterilization process was applied, resulting in accelerated formation of the biomorphic crystals. Briefly, the coating samples were immersed in a small volume of a buffered solution containing 4.2 mM HCO_3^{2-} and subjected to an autoclave sterilization process. The pH value of the buffer is similar to that of human blood plasma. As expected, this hydrothermal condition accelerated crystallization on the coating surface, leading to generation of a three-dimensional porous scaffold built by variously shaped crystals (Figure 1c−f). This scaffold

Received: September 9, 2015
Accepted: October 9, 2015
Published: October 12, 2015

DOI: 10.1021/acsami.5b08493
ACS Appl. Mater. Interfaces 2015, 7, 23412−23417

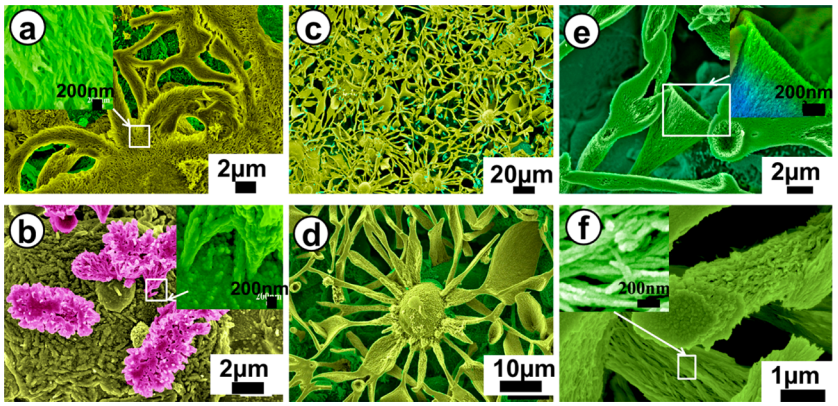

Figure 1. SEM images of the SZnS coatings: (a) after 5 h of incubation in a cell culture medium with 10% FBS; (b) after 5 h of incubation in a cell culture medium without FBS; (c–f) after autoclave treatment (121 °C) for 20 min.

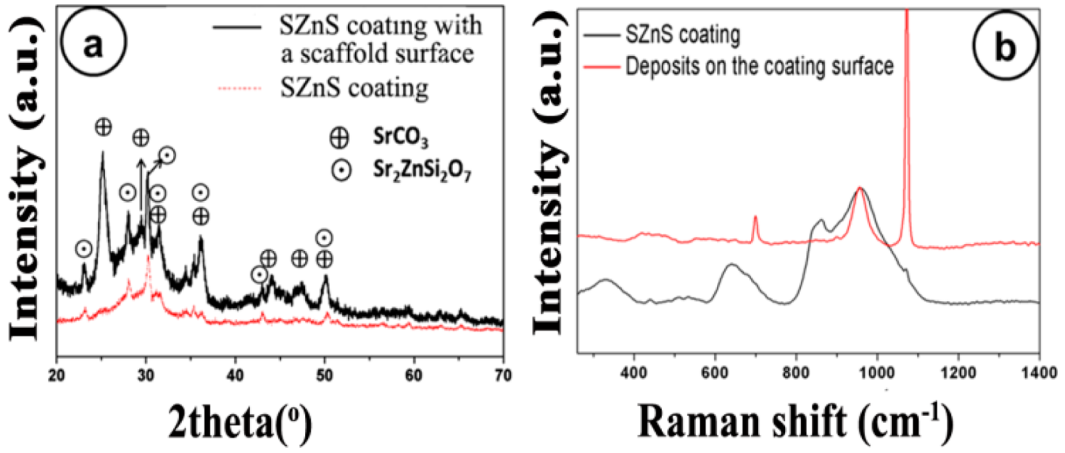

Figure 2. XRD patterns (a) and Raman spectra (b) of the SZnS coating and the coating with a scaffold surface composed of crystals.

covers the whole surface of the coating, providing mechanical and structural support for the seeded osteoblasts. In a magnified view (Figure 1d), it can be clearly seen that the stem or leaflike crystals grow out from the coating surface. Some crystals exhibit an interesting hollow structure, looking like a trumpet (Figure 1e). Under an even higher magnification, we can observe that the crystals are composed of ~50 nm-thick fibrous crystallites (Figure 1f), which is a typical feature of the silica carbonate biomorphs.[1,11] The size of the fibrous crystallites is similar to that of the cellular filopodium, a membrane protrusion of cells for sensing the surrounding environment.[12] In addition, it should be stressed that crystals on low land areas (the valley) and upland areas (the ridge and island) grow in different directions. Those on the lower ground normally grow vertically along a direction perpendicular to the surface (green triangle), while those on the islands grow laterally, forming a chrysanthemum flowerlike structure (Figure S3, blue line patterns). However, no crystals grow on the most elevated areas on the high land (circled by red lines). In the bone regeneration field, it is a promising trend to mimick the nanostructure of the bone matrix to enhance bone regeneration, and the beneficial effects of hybrid micro/nanostructures have been well-documented.[13] Therefore, the in situ formed scaffold on the coating surface exhibiting a structural hierarchy similar to that of the bone extracellular matrix is expected to have a positive effect on the functioning of osteoblasts.

The phase composition of the crystals was confirmed by Raman spectromicroscopy, X-ray diffraction (XRD), and transmission electron microscopy (TEM). Some new diffraction peaks assigned to $SrCO_3$ (PDF 05-0418), not present in the pattern of the as-sprayed coatings, were found in the pattern of the coating with a scaffold surface (Figure 2a), indicating that the newly formed crystals are $SrCO_3$. Obvious differences are also found between the Raman spectra of the as-sprayed coating and the biomorphic crystals formed on the coating surface (Figure 2b). Because of the poor crystallization of the as-sprayed coating (Figure S1), the bands in its Raman spectrum are broad. However, the bands in the spectrum of the crystals formed on the coating surface are sharp, indicating their high crystallinity. All bands in the spectrum of the as-sprayed coating can be assigned to silicate structural units of the SZnS.[14−16] However, a new band, the symmetric stretching band of the carbonate group (CO_3^{2-}), is observed at 1071.8 cm^{-1} in the spectrum of the biomorphic crystals. The symmetric stretching mode of carbonates is strongly dependent on the ionic radius of the cationic ions. The location of the symmetric stretching band in the spectrum of the crystals perfectly matches that of the carbonate group binding to strontium ions (Sr^{2+}).[17] The other band located at ~700 cm^{-1} can also be assigned to the carbonate group.[17]

High-resolution TEM (HRTEM) images of the crystals are shown in Figure 3a. Interplanar distances (d) of ~0.300 and 0.256 nm are found in lattice fringes (Figure 3a), which correspond to the spacing of the 002 and 200 lattice planes of $SrCO_3$ crystals, respectively. Element compositions of the crystals were measured by energy-dispersive spectroscopy

DOI: 10.1021/acsami.5b08493
ACS Appl. Mater. Interfaces 2015, 7, 23412−23417

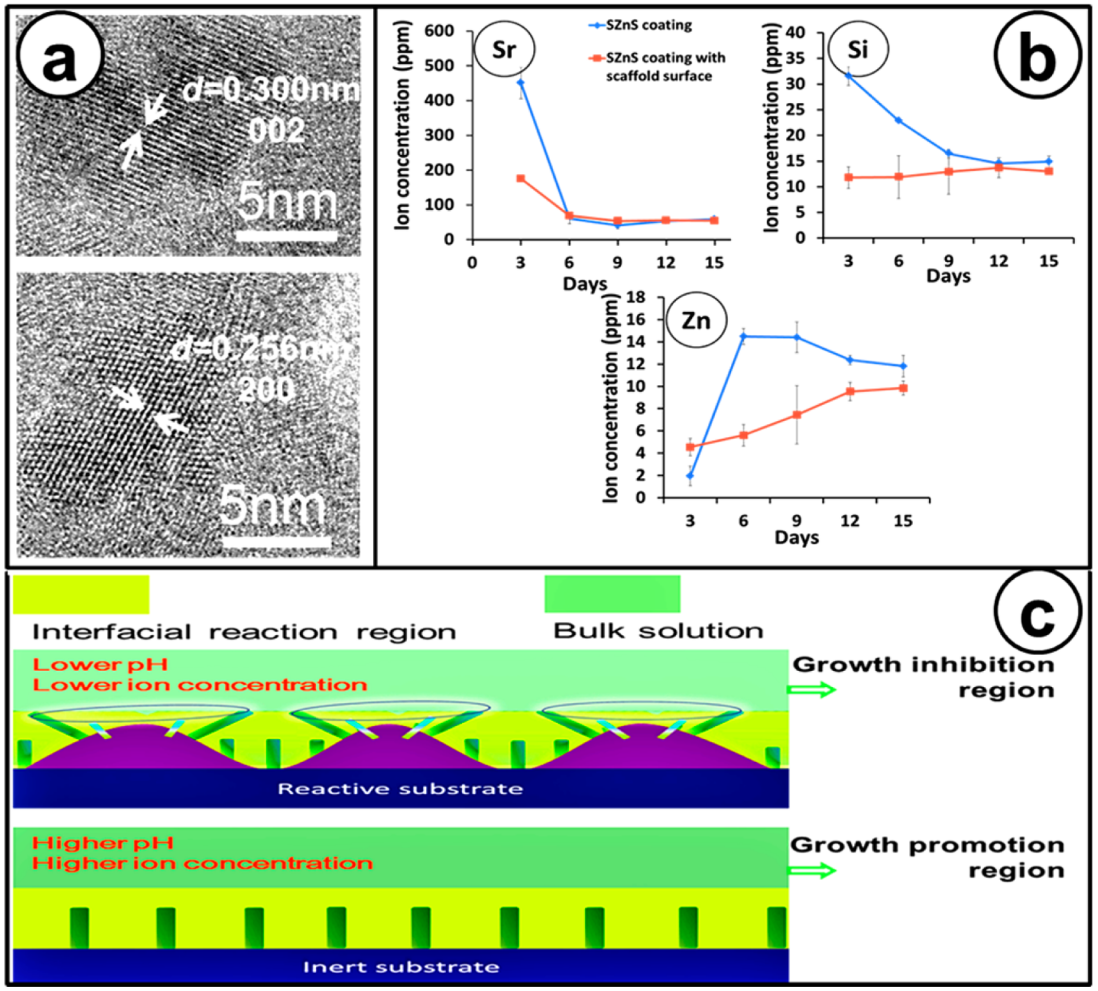

Figure 3. HRTEM image of the crystals formed on the SZnS coating after autoclave treatment (a), ion dissolution profile from the as-sprayed coating and the coating with a crystal scaffold surface (b), and schematic map showing the difference in crystal formation between the traditional and interfacial reaction-driven approaches (c).

(EDS) in conjunction with scanning electron microscopy (SEM) and TEM. Results show that the ratio of Si/Sr for different crystals varies in the range of 0.1:0.4, indicating the coexistence of silica and $SrCO_3$ in the crystals. Figure 3b displays the ion release profiles of the as-sprayed coating and the coating with a crystal scaffold surface. For the as-sprayed coating, a burst release of Sr and Si ions is found in the first 3 days, while the burst release of Zn is observed at day 6. By contrast, the release of the ions from the coating with a scaffold surface is much more constant without large fluctuations, proving that the scaffold layer can prevent the burst release of ions. Because of the well-documented beneficial effects of Sr, Zn, and Si on the activation of bone cell functions and promotion of new bone tissue formation at fracture sites,[18−20] dissolution of the SZnS material is required for bone regeneration applications. However, high reactivity leads to a burst release of their compositional ions, resulting in an excessive dosage and an undesired large fluctuation of the pH from the physiological level caused by the released alkaline-earth metal ions (e.g., Ca, Sr, etc.).[19,21,22] This is a general concern for most of the degradable bioinorganic materials. Therefore, it is crucial to control the initial interfacial chemical interaction to avoid the burst release of ions. The success in the prevention of the burst ion release by the biomorphic crystal scaffold implies the potential use of biomorphic crystals in bone tissue engineering.

As indicated by Figure 3b, Sr ions are preferentially (nonstoichiometrically) released from the SZnS coating, resulting in a negatively charged Si-rich layer on the coating surface and a localized microenvironment with a high pH value.[23] This incongruent dissolution has been found in many silicate glasses and ceramics.[24,25] The Si-rich layer first traps the positively charged Sr ions, which later on bond with CO_3^{2-} groups from the diffusion of carbon dioxide in the atmosphere or from the buffer solution, thus leading to the nucleation of $SrCO_3$. The consumption of CO_3^{2-} leads to the dissociation of nearby HCO_3^- ions, which, in turn, leads to the release of protons and the local reduction of the pH at the crystal growth front. The local drop of the pH causes the polymerization of silicate ions by reacting with H^+ around the just-formed $SrCO_3$ crystallites. As a consequence, the crystallites are coated with a thin siliceous skin, and further growth is inhibited. As the silica polymerization proceeds, the local pH value is reincreased because of the consumption of H^+. Therefore, this proton- or pH-driven autocatalytic cycle ensures the growth of hierarchical biomorphic crystals along a particular direction through the interplay of $SrCO_3$ and amorphous SiO_2 precipitation.[5,26]

The differences of our methodology for producing a silica biomorph from conventional production procedures are

DOI: 10.1021/acsami.5b08493
ACS Appl. Mater. Interfaces 2015, 7, 23412−23417

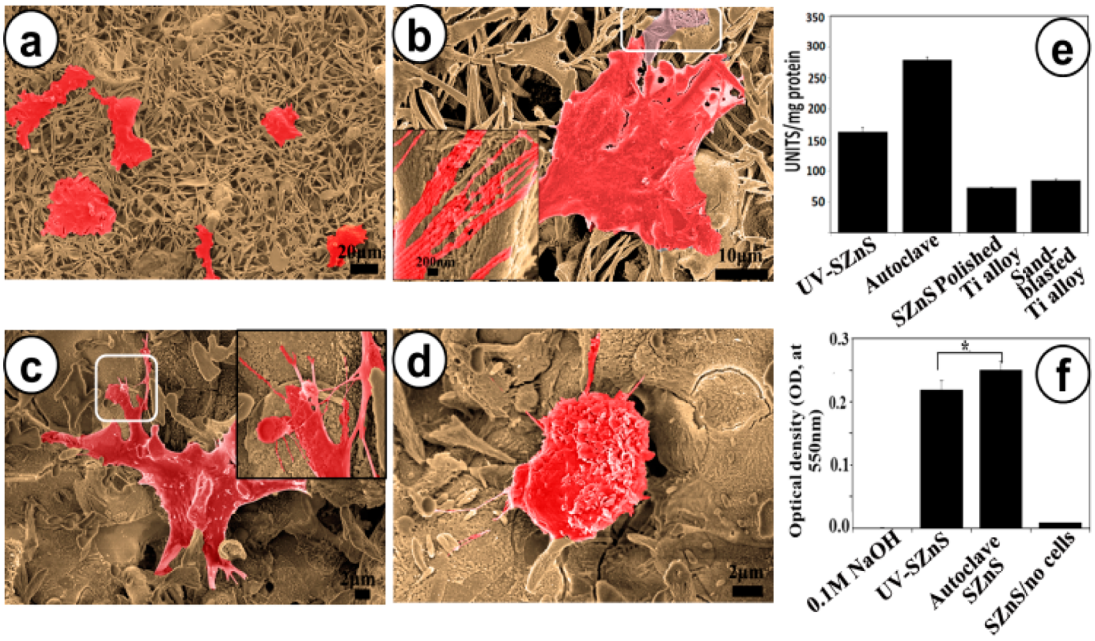

Figure 4. SEM images of osteoblasts cultured on the SZnS coatings with a scaffold surface (a and b) and the as-sprayed coating (c and d). ALP activity (e) and collagen production (f) in the osteoblasts cultured for 14 days on the coating surface.

summarized below, which possibly account for the different morphogenesis of the $SrCO_3$ biomorph in our study. Figure 3c shows a schematic map of the silica-biomorph formation process investigated in this study in comparison with the conventional process. In the conventional process, the substrate used is inert; thus, its existence has no significant influence on the formation of crystals (nucleation and growth). In regions near the substrate surface (yellow colored), the pH and ion concentrations have fluctuations due to the coprecipitation of $SrCO_3$ and SiO_2, while those in the bulk solution are relatively stable and higher than that at the interface. In this case, the bulk solution promotes crystal growth because the higher pH value inhibits SiO_2 precipitation, so that the crystal grows toward/into the bulk solution in a direction perpendicular to the substrate surface. However, the situation is reversed in the case of the interfacial reaction-driven formation investigated in this study. The substrate acts as a reservoir of ions, thus having a strong influence on the localized pH in the interfacial reaction region. Because of the preferential (nonstoichiometric) release of Sr, the pH in the very near surface of the substrate (yellow colored) is higher than that of the bulk solution. Thereby, a more alkaline microenvironment is created between the low ground and the ridges/islands because of the more confined and restricted space, promoting crystal growth. In contrast, the lower pH condition in the bulk solution inhibits crystal growth by favoring SiO_2 formation. Therefore, in low-lying areas, the crystals grow upward until reaching the low-pH bulk solution. However, on the surface of the islands, the crystals laterally project toward the surrounding high-pH microenvironment, instead of growing along the same direction of the crystals in the low-lying areas. With a closer observation, we can see that some glassy materials appeared mostly on top of the stem-shaped crystals and the face-up top part of the leaflike crystals (Figure S4). In back-scattering electron images, the glassy material shows a darker color compared to the fibrous crystallites because the atomic weight of Si (28.08) is much lower than that of Sr (87.62). This finding proves our deduction mentioned above. The glassy layer prevents the further upward growth of the biomorphs. Therefore, the growth of the biomorph crystals in both areas is confined in the reaction region, a "limited" three-dimensional space between the coating surface and bulk solution.

To evaluate the interfacial biological activity of the SZnS coatings with a scaffold surface and the as-sprayed one, MC3T3-E1 osteoblasts were seeded on the coating surface and incubated for 5 h. The morphology of the cells after incubation is presented in Figure 4a,b. All of the cells fully flatten and grow on the scaffold surface with many protrusions from the cell body (Figure 4a,b). In a highly magnified image (Figure 4b), it can be seen that many nanosized fibrous protrusions extend to the neighboring crystals. Upon further closer observation, it was found that the fibrous protrusion is similar to the fibrous crystallites in the leaflike crystals in terms of both size and shape (inset in Figure 4b). Cells cultured on the as-sprayed coating sterilized by UV irradiation show two different representative morphologies. One of them is a normal flattened shape with lamellipodia and filopodia interacting at nanoscale with the substrate, as shown in the inset in Figure 4c. The other is a round but shriveled shape (Figure 4d) with few protrusions. The shrinking of the cells indicates that the coating has a certain degree of harmful effects on the initial attachment and adhesion of the osteoblasts. In addition, we also see some crystals formed during the incubation with cells (Figure 4c,d). The alkaline phosphatase (ALP) activity and collagen production in the osteoblasts, two important indicators of the osteoblastic activity, were also quantitatively evaluated. From Figure 4e,f, it can be seen that the ALP activity and collagen of the osteoblasts cultured on the coating with biomorphic crystals are higher than those cultured on the "bare" surface of the as-sprayed coating, indicating that the scaffold surface enhanced the functions of the osteoblasts, which is possibly ascribed to the joint contribution of the elimination of the burst release of ions and the topographical effects of the hierarchically structured biomorph scaffold. Primary studies were also

DOI: 10.1021/acsami.5b08493
ACS Appl. Mater. Interfaces 2015, 7, 23412−23417

conducted to investigate the interfacial biological reactivity of the SZnS porous scaffolds prepared by a foam impregnation method. Many interesting biomorphs with various shapes were found after incubation with the osteoblasts in a cell culture medium (shown in Figure S5), further evidencing the ability of SZnS to induce the formation of silica biomorphs. A comprehensive investigation into the detailed mechanism behind this interfacial reaction-driven biomorph formation process will be carried out, with the ultimate objective of being able to manually monitor the morphogenesis.

In summary, we present a novel approach to in situ grow silica−strontium carbonate ($SrCO_3$) biomorphs with hierarchical micro/nanostructures on biomedical coatings. The growth of crystals occurs in reversed spatial gradients of the pH and ions (nutrients) compared to those crystals formed in the conventional process. Therefore, the growth of the $SrCO_3$ crystals is confined to a limited space near the SZnS coating surface, where the pH is higher than that of the bulk solution. The formed long leaflike and stem-shaped $SrCO_3$ crystals not only prevent the burst release of ions but also present a hierarchical topography with structural features down to subcellular levels, thus enhancing osteoblast adhesion, upregulating the ALP activity, and increasing collagen production in osteoblasts.

■ ASSOCIATED CONTENT

Supporting Information

The Supporting Information is available free of charge on the ACS Publications website at DOI: 10.1021/acsami.5b08493.

Experimental section, XRD patterns of the ceramic powders for plasma spraying and the as-sprayed coating, surface morphology of the as-sprayed coating, and SEM images of the biomorphic crystals formed on the surface of the coating and the three-dimensional porous scaffold (prepared by a foam-impregnation method) (PDF)

■ AUTHOR INFORMATION

Corresponding Author

*E-mail: gc.wang@siat.ac.cn. Tel.: +86-755-86392561.

Notes

The authors declare no competing financial interest.

■ ACKNOWLEDGMENTS

The authors want to thank the Shenzhen Peacock Innovation Team (Grant 110811003586331) and Shenzhen Key Laboratory of Marine Biomedical Materials (Grant ZDSY20130401165820356) for their support. S.E.M. thanks the National Natural Science Foundation of China (Grant 51120135001) and the Spanish Ministry of Economy (MINECO; Grant MAT2013-48169R).

■ REFERENCES

(1) Kunz, W.; Kellermeier, M. Beyond Biomineralization. *Science* **2009**, *323*, 344−345.

(2) Kellermeier, M.; Melero-García, E.; Glaab, F.; Eiblmeier, J.; Kienle, L.; Rachel, R.; Kunz, W.; García-Ruiz, J. M. Growth Behavior and Kinetics of Self-Assembled Silica-Carbonate Biomorphs. *Chem. - Eur. J.* **2012**, *18* (8), 2272−2282.

(3) García-Ruiz, J. M.; Hyde, S. T.; Carnerup, A. M.; Christy, A. G.; Kranendonk, M. J.; Van Welham, N. J. Self Assembled Silica-Carbonate Structures and Detection of Ancient Microfossils. *Science* **2003**, *302*, 1194−1197.

(4) Kellermeier, M.; Melero-García, E.; Glaab, F.; Klein, R.; Drechsler, M.; Rachel, R.; García-Ruiz, J. M.; Kunz, W. J. Stabilization of Amorphous Calcium Carbonate in Inorganic Silica-Rich Environments. *J. Am. Chem. Soc.* **2010**, *132* (50), 17859−17866.

(5) Noorduin, W. L.; Grinthal, A.; Mahadevan, L.; Aizenberg, J. Rationally Designed Complex, Hierarchical Microarchitectures. *Science* **2013**, *340* (6134), 832−837.

(6) Eiblmeier, J.; Kellermeier, M.; Deng, M.; Kienle, L.; García-Ruiz, J. M.; Kunz, W. Bottom-Up Self-Assembly of Amorphous Core-Shell-Shell Nanoparticles and Biomimetic Crystal Forms in Inorganic Silica-Carbonate Systems. *Chem. Mater.* **2013**, *25* (9), 1842−1851.

(7) Fan, T. X.; Chow, S. K.; Zhang, D. Biomorphic Mineralization from Biology to Materials. *Prog. Mater. Sci.* **2009**, *54* (5), 542−659.

(8) Wang, Q.; Wang, Y. Y.; Guo, X. Y. Biomorphic High-Performance Materials. *Prog. Chem.* **2007**, *19* (7−8), 1217−1222.

(9) Kellermeier, M.; Gebauer, D.; Melero-García, E.; Drechsler, M.; Talmon, Y.; Kienle, L.; Cölfen, H.; García-Ruiz, J. M.; Kunz, W. Colloidal Stabilization of Calcium Carbonate Prenucleation Clusters with Silica. *Adv. Funct. Mater.* **2012**, *22* (20), 4301−4311.

(10) García-Ruiz, J. M.; Melero-García, E.; Hyde, S. T. Morphogenesis of Self-Assembled Nanocrystalline Materials of Barium Carbonate and Silica. *Science* **2009**, *323* (5912), 362−365.

(11) Terada, T.; Yamabi, S.; Imai, H. Formation Process of Sheets and Helical Forms Consisting of Strontium Carbonate Fibrous Crystals with Silicate. *J. Cryst. Growth* **2003**, *253* (1−4), 435−444.

(12) Jacquemet, G.; Hamidi, H.; Ivaska, J. Filopodia in Cell Adhesion, 3D Migration and Cancer Cell Invasion. *Curr. Opin. Cell Biol.* **2015**, *36*, 23−31.

(13) Kane, R.; Ma, P. X. Mimicking the Nanostructure of Bone Matrix to Regenerate Bone. *Mater. Today* **2013**, *16* (11), 418−423.

(14) Kothiyal, G. P.; Goswami, M.; Tiwari, B.; Sharma, K.; Ananthanarayanan, A.; Montagne, L. Some Recent Studies on Glass/Glass-Ceramics for Use as Sealants with Special Emphasis for High Temperature Applications. *J. Adv. Ceram.* **2012**, *1* (2), 110−129.

(15) Sharma, S. K.; Yoder, H. S.; Matson, D. W. Raman Study of Some Melilites in Crystalline and Glassy States. *Geochim. Cosmochim. Acta* **1988**, *52* (8), 1961−1967.

(16) Tiwari, B.; Gadkari, S. C.; Kothiyal, G. P. Investigation on Glasses in Strontium Zinc Borosilicate System as Sealants for Solid Oxide Fuel Cell. *Adv. Mater. Res.* **2012**, *585*, 195−199.

(17) Kaabar, W.; Bott, S.; Devonshire, R. Raman Spectroscopic Study of Mixed Carbonate Materials. *Spectrochim. Acta, Part A* **2011**, *78* (1), 136−141.

(18) Zhao, L.; Wang, H.; Huo, K.; Zhang, X.; Wang, W.; Zhang, Y.; Wu, Z.; Chu, P. K. The Osteogenic Activity of Strontium Loaded Titania Nanotube Arrays on Titanium Substrates. *Biomaterials* **2013**, *34* (1), 19−29.

(19) Zhang, W.; Wang, G.; Liu, Y.; Zhao, X.; Zou, D.; Zhu, C.; Jin, Y.; Huang, Q.; Sun, J.; Liu, X.; Jiang, X.; Zreiqat, H. The Synergistic Effect of Hierarchical Micro/Nano-Topography and Bioactive Ions for Enhanced Osseointegration. *Biomaterials* **2013**, *34*, 3184−3195.

(20) Hoppe, A.; Güldal, N. S.; Boccaccini, A. R. A review of the Biological Response to Ionic Dissolution Products from Bioactive Glasses and Glass-Ceramics. *Biomaterials* **2011**, *32* (11), 2757−2774.

(21) Lao, J.; Nedelec, J. M.; Jallot, E. New Strontium-Based Bioactive Glasses: Physicochemical Reactivity and Delivering Capability of Biologically Active Dissolution Products. *J. Mater. Chem.* **2009**, *19* (19), 2940.

(22) Soulié, J.; Nedelec, J. M.; Jallot, E. Influence of Mg Doping on the Early Steps of Physico-Chemical Reactivity of Sol-Gel Derived Bioactive Glasses in Biological Medium. *Phys. Chem. Chem. Phys.* **2009**, *11* (44), 10473−10483.

(23) Wu, C.; Chang, J. A Review of Bioactive Silicate Ceramics. *Biomed. Mater.* **2013**, *8*, 032001.

(24) Wang, G. C.; Lu, Z. F.; Dwarte, D.; Zreiqat, H. Porous Scaffolds with Tailored Reactivity Modulate in-vitro Osteoblast Responses. *Mater. Sci. Eng., C* **2012**, *32* (7), 1818−1826.

DOI: 10.1021/acsami.5b08493
ACS Appl. Mater. Interfaces 2015, 7, 23412−23417

(25) Wang, G. C.; Lu, Z. F.; Liu, X. Y.; Zhou, X. M.; Ding, C. X.; Zreiqat, H. Nanostructured Glass-Ceramic Coatings for Orthopaedic Applications. *J. R. Soc., Interface* **2011**, *8* (61), 1192−1203.
(26) Kellermeier, M.; Melero-García, E.; Kunz, W.; García-Ruiz, J. M. Local Autocatalytic Co-Precipitation Phenomena in Self-Assembled Silica-Carbonate Materials. *J. Colloid Interface Sci.* **2012**, *380* (1), 1−7.

DOI: 10.1021/acsami.5b08493
ACS Appl. Mater. Interfaces 2015, 7, 23412−23417